J. Fluid Mech. (2006), *vol.* 554, *pp.* 147–166. © 2006 Cambridge University Press
doi:10.1017/S0022112006009268 Printed in the United Kingdom

Solidification of colloidal suspensions

By S. S. L. PEPPIN[1], J. A. W. ELLIOTT[2] AND M. GRAE WORSTER[1]

[1]Institute of Theoretical Geophysics, Department of Applied Mathematics and Theoretical Physics, University of Cambridge, Wilberforce Road, Cambridge CB3 0WA, UK

[2]Department of Chemical and Materials Engineering, University of Alberta, Edmonton, Canada, T6G 2G6

(Received 2 February 2005 and in revised form 30 January 2006)

We present a mathematical model of the unidirectional solidification of a suspension of hard-sphere colloids. Similarity solutions are obtained for the volume fraction and temperature profiles ahead of a planar solidification front. The highly nonlinear functional dependence of the diffusion coefficient on the volume fraction gives rise to a range of behaviours. For small particles, Brownian diffusion dominates and the system behaviour is reminiscent of binary-alloy solidification. Constitutional supercooling occurs at the interface under certain conditions, leading potentially to an instability in the shape of the interface. For larger particles, Brownian diffusion is weak and the particles form a porous layer above the interface. In this case constitutional supercooling reaches a maximum near the surface of the layer, and the porous medium itself is potentially unstable. In stable systems there exists the possibility of secondary nucleation of ice.

1. Introduction

In the material, soil, biological and food sciences it is often necessary or desirable to solidify a suspension of particles. Examples include the fabrication of composite materials, the freezing of soils, and the preservation of cells, tissues and perishable foods. The problem has been studied for many years from the point of view of a single particle interacting with an advancing solidification front. Theories have been developed capable of predicting conditions under which an isolated particle will be pushed ahead of and/or engulfed by the interface (Uhlmann, Chalmers & Jackson 1964; Chernov, Temkin & Mel'nikova 1976; Rempel & Worster 1999). In many systems, a concentrated layer of particles builds up against the interface (Mashl, Flores & Trivedi 1996; Mutou *et al.* 1998; Muldrew *et al.* 2000; Zhang *et al.* 2005). This is illustrated in figure 1, which shows the results of some of our own experiments on the freezing of clay suspensions in water. At slow freezing rates all the clay particles are excluded from the growing ice and a concentrated layer forms above the solidification front (figure 1*a*). At faster freezing rates, the ice forms a dendritic layer, presumably in consequence of a morphological instability of the ice front (figure 1*b*). This behaviour is reminiscent of the solidification of binary alloys (Mullins & Sekerka 1964; Kurz & Fisher 1986; Huppert 1990; Worster 2000). More exotic behaviour can occur at different particle concentrations and freezing rates. One example is shown in figure 1(*c*), in which a polygonal structure of pure ice lenses has formed during solidification. The particles in the concentrated suspension interact with each other and the system cannot be modelled on the basis of isolated-particle theories. Many

https://doi.org/10.1017/S0022112006009268 Published online by Cambridge University Press

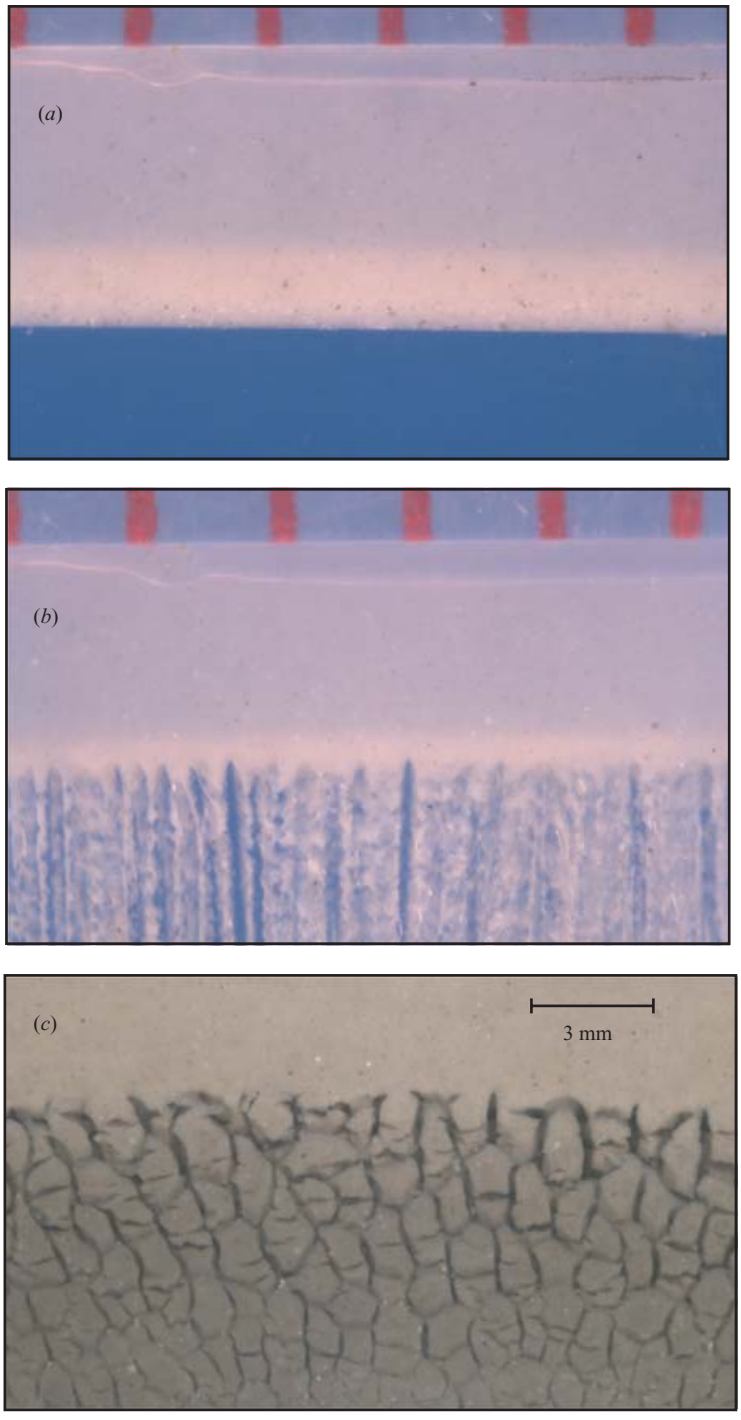


FIGURE 1. Unidirectional solidification of montmorillonite clay (5 wt% suspended in water, pH 10), performed by cooling the base of the cell to a set temperature T_b. The cooling plate is positioned approximately 1 cm below the field of view. In (*a*) the solidification rate is slow ($T_b \approx -3\,^{\circ}\mathrm{C}$). The interface remains planar and rejects all of the particles, leaving behind a layer of pure ice (in blue). In (*b*) the solidification is faster ($T_b \approx -20\,^{\circ}\mathrm{C}$). The interface has become unstable, forming dendritic structures. The gradations at the top of the figures are in millimetres. In (*c*) the concentration has been increased to 50 wt%, and the ice forms a polygonal pattern. The temporal development of these systems is shown in movies 1–3 available with the online version of this paper.

https://doi.org/10.1017/S0022112006009268 Published online by Cambridge University Press

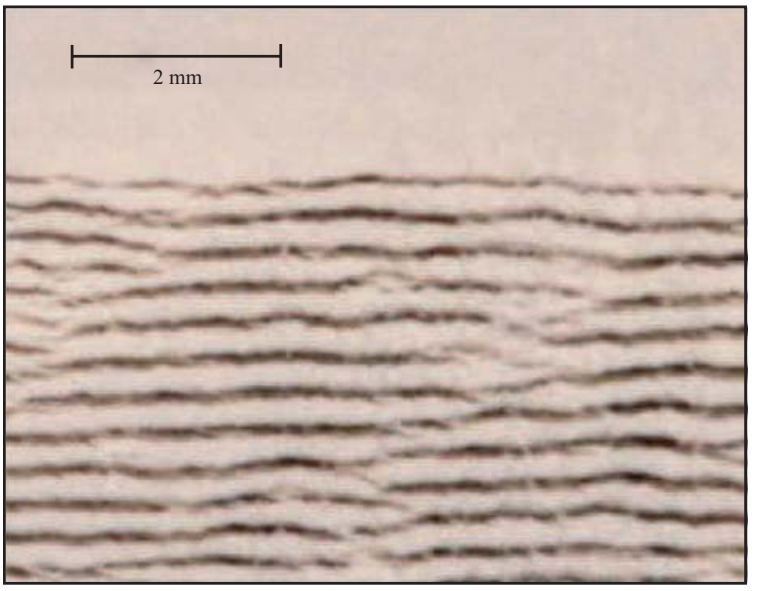


FIGURE 2. Unidirectional solidification of kaolinite clay (60 wt% suspended in water, pH 9), performed by translating the cell at $1\,\mu m\,s^{-1}$ through a fixed temperature gradient ($3^{\circ}cm^{-1}$). A series of planar ice lenses (dark regions) has formed in the clay, with the thickness of the lenses depending on the initial clay concentration as well as on the translation speed.

different physical interactions occur in these systems, involving intermolecular forces between the different phases, viscous fluid flow and possibly electro-phoretic processes, depending on the variations in ionic concentrations within the suspension phase. In this paper we begin the development of a continuum model of such systems that can be used to analyse these different situations.

Yet another type of behaviour was observed by Mutou *et al.* (1998). They froze a suspension of silica spheres by pulling a sample through a constant temperature gradient. As the solidification progressed, a layer of particles accumulated ahead of the freezing front in a process similar to the development of a filter cake (the concentrated layer collected against a filter by pressure-driven flow of a fluid suspension) and the situation shown in figure 1(*a*). Eventually a new layer of ice formed ahead of the concentrated layer of particles. The process then repeated, creating a banded structure in the solid (Mutou *et al.* 1998; Watanabe 2002). This phenomenon is illustrated in figure 2 which shows the result of pulling a concentrated suspension of kaolinite through a fixed temperature gradient, yielding a series of planar ice lenses. Similar phenomena occur in tissue, concrete, soils and many other materials (Taber 1929; Scherer 1993; Muldrew *et al.* 2000; Corr, Monteiro & Bastacky 2003).

Previous approaches to the study of ice lenses have generally treated the soil as a rigid porous medium consisting of non-colloidal particles (O'Neill & Miller 1985; Rempel, Wettlaufer & Worster 2004). One of the assumptions of these models is the existence of a *frozen fringe*, a region of partially frozen soil beyond the warmest ice lens (Miller 1972). Recent experiments on a soil consisting of uniform silica spheres were unable to detect a frozen fringe (Watanabe & Mizoguchi 2000; Watanabe, Muto & Mizoguchi 2001). In the present work we begin from an alternative point of view, and propose mechanisms for these ice formations based on our understanding of the freezing of colloidal systems.

https://doi.org/10.1017/S0022112006009268 Published online by Cambridge University Press

In preparation for this we review and extend some classical results on the dynamics and thermodynamics of suspensions of hard-sphere colloids. We obtain in § 2 a general expression for the mass flux in a hard-sphere suspension. We also obtain expressions for the osmotic pressure, diffusion coefficient and freezing temperature (§ 4.2). In § 3 we calculate the volume fraction and pressure profiles during the filtration of a hard-sphere suspension over a range of particle sizes and flow rates. These profiles illustrate the approach we take to modelling solidification in later sections. Two limiting types of behaviour are seen. For small particles, Brownian diffusion is relatively strong and the particles form a diffuse boundary layer against the filter surface; for large particles, Brownian diffusion is negligible and the particles form a close-packed porous medium.

In § 4 we present an extended Stefan model of the solidification of a hard-sphere suspension, and determine similarity solutions for the volume fraction and temperature profiles. Depending on the particle size and solidification rate, similar limiting behaviours are found as in the case of filtration. For small particles a diffuse boundary layer forms against the freezing front. If the flat interface advances too rapidly, constitutional supercooling can occur in the suspension, and the interface is potentially unstable. For larger particles, a porous medium forms ahead of the solidification front. The suspension ahead of the porous medium can become supercooled. The maximum in supercooling occurs at the surface of the porous medium, allowing for the possibility of secondary nucleation of ice.

2. Mass flux in a hard-sphere suspension

When a mixture solidifies, it is typical that certain components of the mixture are preferentially incorporated within the solid phase. The progress of solidification is then dictated in large part by the transport of the other components away from the solidification front. In this section we briefly review continuum descriptions of particulate suspensions in order to determine a convenient representation of mass transport for use in our study of solidification.

We consider a suspension of rigid spherical particles (hard spheres) with radius R and constant density ρ_p. An equation describing the motion of the spheres relative to the suspending medium (Batchelor 1976; Davis & Russel 1989; Peppin, Elliott & Worster 2005) is

$$\frac{6\pi R\mu}{f}(\boldsymbol{v}_2 - \boldsymbol{v}) = -\frac{1}{n}\nabla\Pi + \boldsymbol{K}. \tag{2.1}$$

Here μ is the dynamic viscosity of the intervening fluid and $6\pi R\mu$ is the Stokes resistance of an isolated sphere. The dimensionless friction factor $f(n)$ accounts for the effect of particle–particle interactions on the viscous resistance, where

$$n = \frac{\phi}{v_p} = \frac{\rho_2}{m_p} \tag{2.2}$$

is the number of particles per unit volume. Here ϕ is the local volume fraction and ρ_2 the partial mass density of the particles, $v_p = \frac{4}{3}\pi R^3$ is the volume of a particle, and $m_p = v_p\rho_p$ the particle mass. The quantity

$$\boldsymbol{v} = (1-\phi)\boldsymbol{v}_1 + \phi\boldsymbol{v}_2 \tag{2.3}$$

in (2.1) is the volume-averaged velocity of the mixture, while $\boldsymbol{v}_1$ and $\boldsymbol{v}_2$ are respectively the average velocities of the suspending liquid and particles relative to the laboratory

https://doi.org/10.1017/S0022112006009268 Published online by Cambridge University Press

frame. The force $\boldsymbol{K} = v_p(\rho_p - \rho_f)\boldsymbol{g}$ is the net gravitational force acting on each particle, where ρ_f is the density of the fluid (assumed constant) and $\boldsymbol{g}$ is the acceleration due to gravity.

The quantity Π is the osmotic pressure of the suspension, defined by the equation

$$\Pi \equiv P - p, \tag{2.4}$$

where P is the pressure of the mixture as a whole and p is the *pervadic* pressure of the pure fluid separated from the suspension by a rigid semi-permeable partition (Peppin *et al.* 2005). As noted by Batchelor and others (Batchelor 1976; Auzerais, Jackson & Russel 1988), the osmotic pressure is equivalent to the transmitted stress in a concentrated suspension of particles in which the pervadic pressure is equivalent to the Darcy pressure.

Equation (2.1) expresses the balance of momentum for the components of the mixture (the particles and fluid). Conservation of momentum for the mixture as a whole is described by

$$\nabla P = \rho \boldsymbol{g}, \tag{2.5}$$

where $\rho = (1-\phi)\rho_f + \phi\rho_p$ is the density of the mixture.

In the absence of gravity equation (2.1) can be written in the form of Fick's law

$$\rho_2(\boldsymbol{v}_2 - \boldsymbol{v}) = -\frac{f}{6\pi R\mu}\left(\frac{\partial \Pi}{\partial n}\right)\nabla\rho_2. \tag{2.6}$$

Equation (2.6) states that the mass flux of component 2 is linearly related to its concentration gradient. One can define a diffusion coefficient D (Davis & Russel 1989) by

$$D \equiv \frac{f}{6\pi R\mu}\frac{\partial \Pi}{\partial n}. \tag{2.7}$$

Combining (2.7) with (2.1) yields

$$\rho_2(\boldsymbol{v}_2 - \boldsymbol{v}) = -D\nabla\rho_2 + \rho_2 f\boldsymbol{U}, \tag{2.8}$$

where $\boldsymbol{U} = \boldsymbol{K}/6\pi R\mu$ is the Stokes velocity of an isolated sphere.

With (2.3), (2.4) and (2.5), equation (2.1) can alternatively be written in the form of Darcy's law

$$(1-\phi)(\boldsymbol{v}_1 - \boldsymbol{v}_2) = -\frac{1}{n}\frac{f}{6\pi R\mu}(\nabla p - \rho_f \boldsymbol{g}). \tag{2.9}$$

Equation (2.9) states that the volume flux of component 1 relative to component 2 is a linear function of the quantity $\nabla p - \rho_f \boldsymbol{g}$. One can define a coefficient k (the permeability) such that

$$\frac{k}{\mu} \equiv \frac{1}{n}\frac{f}{6\pi R\mu}. \tag{2.10}$$

Inserting (2.10) into (2.9) yields

$$(1-\phi)(\boldsymbol{v}_1 - \boldsymbol{v}_2) = -\frac{k}{\mu}(\nabla p - \rho_f \boldsymbol{g}). \tag{2.11}$$

Comparing (2.10) with (2.7) shows that

$$D = n\frac{k}{\mu}\frac{\partial \Pi}{\partial n}. \tag{2.12}$$

https://doi.org/10.1017/S0022112006009268 Published online by Cambridge University Press

Equation (2.12), which has appeared several times in the literature (Auzerais *et al.* 1988; Davis & Russel 1989; Petsev, Starov & Ivanov 1993; Peppin *et al.* 2005), relates the transport coefficients D and k to the same underlying physical variables. As we illustrate in § 3, whether one chooses to speak in terms of a diffusion coefficient D or a permeability k depends partly on convention and partly on the closeness of the particular system under consideration to a solution or a porous medium, respectively.

2.1. *Diffusion coefficient*

Given expressions for the osmotic pressure and permeability, equation (2.12) can be used to obtain the diffusion coefficient as a function of volume fraction (Auzerais *et al.* 1988). The osmotic pressure of a suspension of hard spheres can be written as

$$\Pi(\phi) = \frac{\phi}{v_p} k_B T z(\phi) \tag{2.13}$$

(Russel, Saville & Schowalter 1989), where k_B is Boltzmann's constant and T is the absolute temperature. The dimensionless compressibility factor $z(\phi)$ accounts for the effect of particle–particle interactions on the osmotic pressure. The form of (2.13) is based on a fundamental result from statistical mechanics which states that the osmotic pressure of a suspension of particles and the pressure of a pure gas are the same functions of volume fraction as long as the particle–particle interaction potential is the same (McMillan & Mayer 1945; Russel *et al.* 1989; Brady 1993). At low volume fraction the compressibility factor can be expanded in the form of a virial series in the volume fraction as

$$z(\phi) = \sum_{n=0}^{\infty} \beta_n \phi^n. \tag{2.14}$$

The first few coefficients β_n in the series have been obtained via statistical mechanical techniques (Thiele 1963; McQuarrie 1976). At higher concentrations the integrations become intractable and the coefficients are commonly obtained via molecular dynamics simulations (Ree & Hoover 1964; Woodcock 1981; Russel *et al.* 1989). By fitting the results of these simulations, Carnahan & Starling (1969) obtained the approximate expression

$$z(\phi) = \frac{1 + \phi + \phi^2 - \phi^3}{(1-\phi)^3} \qquad (0 \leqslant \phi \lesssim 0.55). \tag{2.15}$$

For $\phi \gtrsim 0.49$, the most stable configuration for a hard-sphere suspension is a crystalline phase (Russel *et al.* 1989; Van Megen, Pusey & Bartlett 1990). However, in colloidal suspensions the hard-sphere crystal is difficult to nucleate and the disordered state persists for $\phi > 0.49$. We discuss this further with regard to the freezing-temperature curve in § 4.2.

Considerations of the free volume available to a disordered system of hard spheres indicate that the pressure should diverge like $(\phi - \phi_p)^{-1}$ as ϕ approaches the random close packing fraction ϕ_p (Woodcock 1981). Molecular dynamics simulations of hard spheres at higher concentrations are in agreement with this prediction, giving

$$z(\phi) = \frac{\alpha}{(\phi_p - \phi)} \qquad (0.55 \lesssim \phi < \phi_p), \tag{2.16}$$

where $\alpha \approx 1.5$ and $\phi_p \approx 0.64$ (Woodcock 1981; Rintoul & Torquato 1996). An expression for $z(\phi)$ that is approximately valid over the entire concentration range

https://doi.org/10.1017/S0022112006009268 Published online by Cambridge University Press

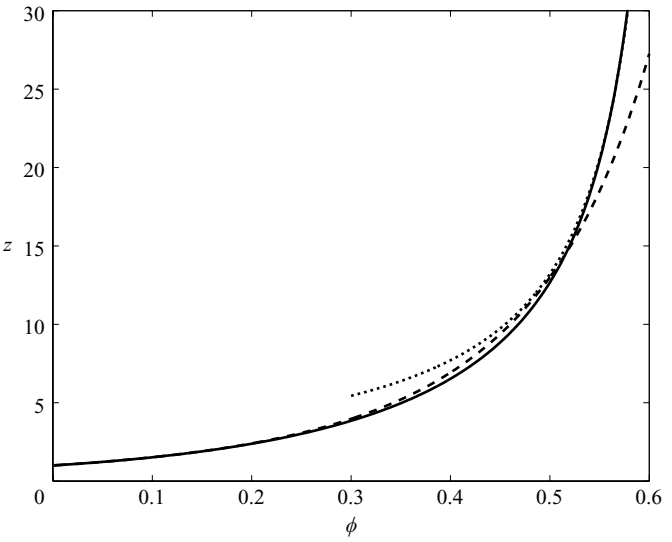


FIGURE 3. Compressibility factor z of a hard-sphere suspension. At low concentration the compressibility factor obeys the Carnahan–Starling equation (2.15) (dashed line). Near close-packing, z diverges according to equation (2.16) (dotted line). The solid line is from equation (2.17).

can be obtained using asymptotic matching to yield

$$z(\phi) = \frac{1 + a_1\phi + a_2\phi^2 + a_3\phi^3 + a_4\phi^4}{1 - \phi/\phi_p}, \tag{2.17}$$

where $a_1 = 4 - 1/\phi_p$, $a_2 = 10 - 4/\phi_p$, $a_3 = 18 - 10/\phi_p$, and $a_4 = \alpha/\phi_p^5 - 18/\phi_p$. The a_k in (2.17) were obtained by expanding the denominators in (2.15) and (2.16), and ensuring that (2.17) agrees with (2.15) to order ϕ^3 as $\phi \to 0$ and with (2.16) to order $(\phi_p - \phi)^{-1}$ as $\phi \to \phi_p$. Expressions (2.15), (2.16) and (2.17) are plotted in figure 3.

For the permeability of a suspension of hard spheres, we use the empirical expression

$$k(\phi) = \frac{2R^2}{9\phi}(1 - \phi)^6, \tag{2.18}$$

which was obtained by Russel *et al.* (1989) by fitting the results of experiments on polystyrene spheres and is shown in figure 4(*a*).

Combining (2.18), (2.17) and (2.13) with (2.12) yields

$$D(\phi) = D_0\hat{D}(\phi), \tag{2.19}$$

where $D_0 = k_BT/6\pi R\mu$ is the Stokes–Einstein diffusivity and

$$\hat{D}(\phi) = (1 - \phi)^6\frac{\mathrm{d}(\phi z)}{\mathrm{d}\phi}. \tag{2.20}$$

The expressions above have the properties (figure 4)

$$D \to D_0 \quad \text{and} \quad k \to \infty \qquad (\phi \to 0),$$

$$D \to \infty \quad \text{and} \quad k \to k(\phi_p) \qquad (\phi \to \phi_p).$$

These limits illustrate why it is more convenient to use Fick's law (2.8) as the constitutive relation for dilute suspensions (D remains finite as $\phi \to 0$ while k

https://doi.org/10.1017/S0022112006009268 Published online by Cambridge University Press

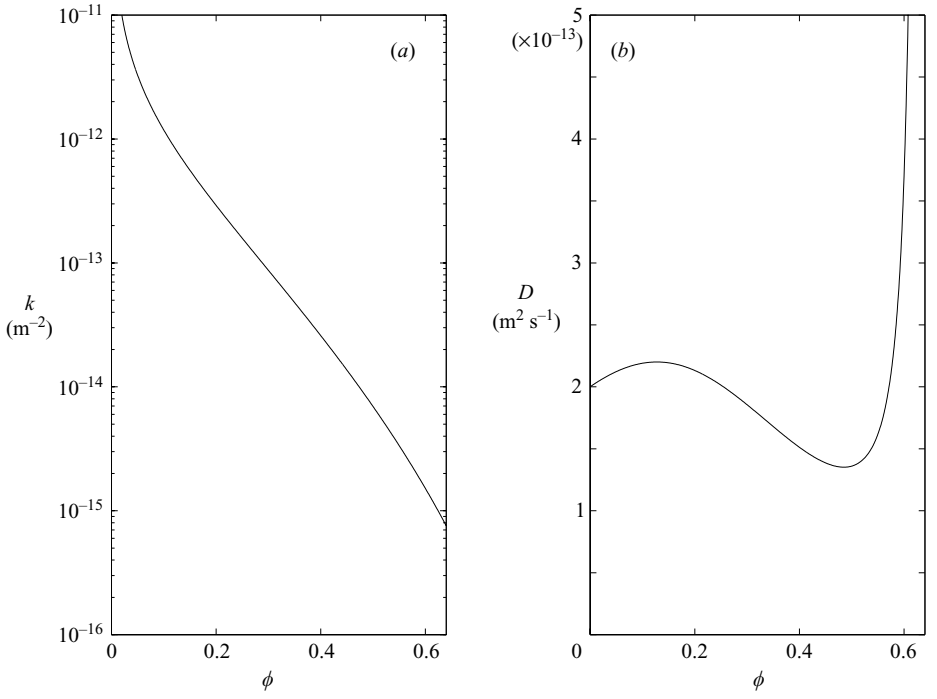


FIGURE 4. (*a*) Permeability $k(\phi)$ and (*b*) diffusion coefficient $D(\phi)$ of a hard-sphere suspension ($R = 10^{-6}$ m), obtained from equations (2.17)–(2.20). The diffusion coefficient decreases at intermediate ϕ owing to viscous effects and diverges near close packing owing to particle-particle interactions (Russel *et al.* 1989). Conversely, the permeability remains finite near close packing but diverges as $\phi \to 0$.

diverges) and Darcy's law (2.11) for close-packed suspensions and porous media (k remains finite as $\phi \to \phi_p$ while D diverges). The mutual diffusion coefficient $D(\phi)$ should, however, be distinguished from the self-diffusivity $D_s(\phi)$ of an individual hard-sphere particle, which approaches zero as $\phi \to \phi_p$ (Rallison 1988; Davis, Russel & Glantschnig 1989). That is, in the close-packed limit the individual particles are not free to diffuse, although the particle matrix as a whole responds rapidly to gradients in volume fraction. Equations (2.19), (2.20) and (2.17) will be used in the following sections to model relative motion in hard-sphere systems over the entire range of volume fraction.

3. Filtration of a hard-sphere suspension

Consider the system in figure 5. Experimentally, a suspension of hard-sphere particles with initial concentration ϕ_0 is placed above a filter to an initial height L. Above the suspension is pure component 1. The filter is rigid and permeable only to component 1. At $t = 0$ a pressure P is applied, initiating a flow of fluid.

3.1. *Conservation of mass*

Conservation of mass in the suspension can be written

$$\frac{\partial(1-\phi)}{\partial t} + \nabla\cdot(1-\phi)\boldsymbol{v}_1 = 0. \tag{3.1}$$

https://doi.org/10.1017/S0022112006009268 Published online by Cambridge University Press

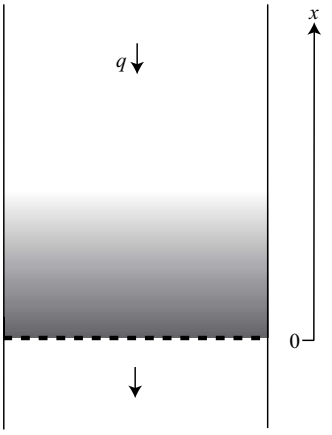


FIGURE 5. Schematic of a steady-state filtration boundary layer. The grey region is a hard-sphere suspension. The white regions signify pure component 1. The sides of the flow cell are assumed frictionless, or far enough away to have no effect on the filtration process.

At steady state, equation (3.1) can be simplified for the one-dimensional system in figure 5 ($\boldsymbol{v}_1 = -v_1\boldsymbol{i}$) to give

$$-\frac{\mathrm{d}q}{\mathrm{d}x} = 0, \tag{3.2}$$

where $q = (1-\phi)v_1$ is the specific discharge of fluid. Thus, q is constant at steady state. Also, at steady state the particles are statistically stationary in the laboratory frame ($\boldsymbol{v}_2 = 0$). Neglecting the effects of gravity, equations (2.8) and (2.11) become, using (2.3),

$$q = -\frac{D(\phi)}{\phi}\frac{\mathrm{d}\phi}{\mathrm{d}x} = \frac{k(\phi)}{\mu}\frac{\mathrm{d}p}{\mathrm{d}x}. \tag{3.3}$$

As noted in § 2, either D or k can be chosen as the relevant transport coefficient. We shall model the system in terms of D and ϕ. The connection between the two approaches will become apparent in § 3.2 when we show that $p(x)$ can be calculated once $\phi(x)$ is known.

Although variations in L and ϕ_0 will change the dynamical approach to steady state, the final configuration depends only on the volume of particles per unit area $\phi_0 L$. Introducing the dimensionless variables $\hat{x} = x/\phi_0 L$ and $\hat{D} = D/D_0$, equation (3.3) becomes

$$Pe\,\phi = -\hat{D}(\phi)\frac{\mathrm{d}\phi}{\mathrm{d}\hat{x}} \qquad (\hat{x} \geqslant 0), \tag{3.4}$$

where $Pe = q\phi_0 L/D_0$ is the Péclet number and $\hat{D}$ is given by equations (2.20) and (2.17). Equation (3.4) can be solved given a boundary condition for ϕ_i, the volume fraction at the filter. This condition can be obtained by integrating (3.4) using overall mass conservation, which leads to

$$\int_0^\infty \phi(\hat{x})\,\mathrm{d}\hat{x} = 1 = -\frac{1}{Pe}\int_{\phi_i}^0 \hat{D}(\phi)\,\mathrm{d}\phi. \tag{3.5}$$

Equation (3.5) ensures that the total number of hard-sphere particles present in the system is conserved. Equation (3.5) can be solved to give an implicit expression

https://doi.org/10.1017/S0022112006009268 Published online by Cambridge University Press

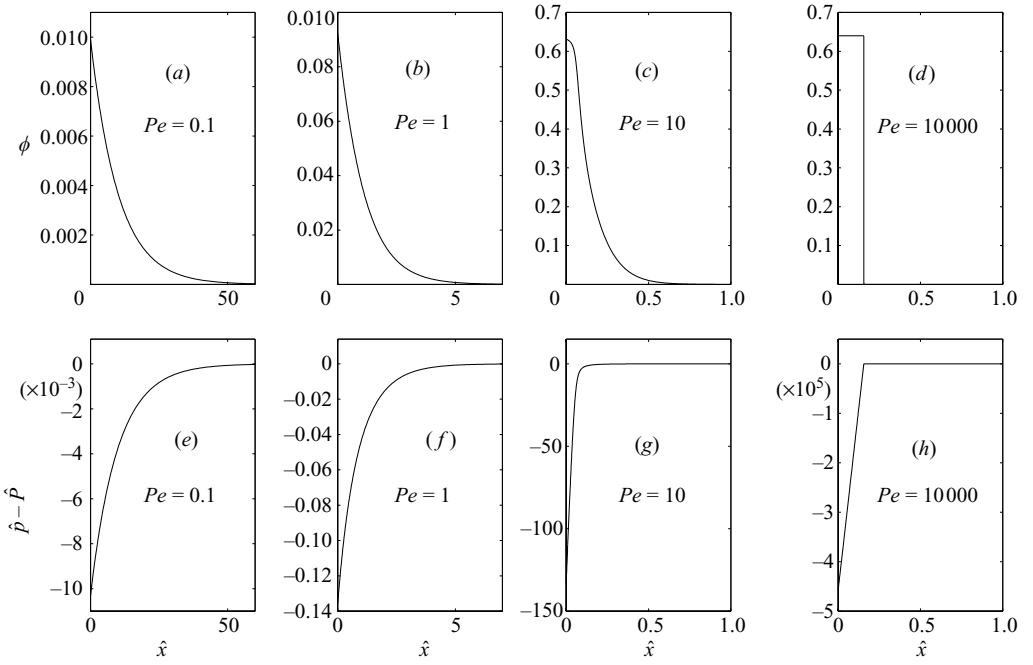


FIGURE 6. Variation in the volume fraction ϕ (*a–d*) and dimensionless pervadic pressure $\hat{p}$ (*e–h*) across a steady-state filtration boundary layer: (*a*) and (*e*) represent the Brownian limit, while (*d*) and (*h*) represent the porous-medium limit. Note the different scales used for the drop in pressure as the Peclet number increases.

for $\phi_i(Pe)$. Equation (3.4) can then be integrated from 0 to $\hat{x}$ to yield an implicit expression for $\phi(\hat{x})$.

3.2. *Filtration profiles*

Figure 6(*a–d*) shows plots of $\phi(\hat{x})$ obtained for increasing Péclet number. In figure 6(*a*) the Stokes–Einstein diffusion velocity $D_0/\phi_0 L$ is larger than the specific discharge q of the fluid, and the concentration profile is influenced mainly by Brownian diffusion. In this case, the concentration decays exponentially away from the filter surface. However, as the flow rate increases or equivalently the particle size increases (so that the diffusivity decreases) Brownian diffusion becomes less important relative to advection, and the particles begin to pile up against the filter surface. Eventually, for $Pe \gg 1$ (figure 6*d*), Brownian diffusion is almost absent and the particles form a close-packed layer of uniform concentration.

Figures 6(*a*)–6(*d*) are similar to volume-fraction profiles obtained by Davis & Russel (1989) in their study of sedimentation and filtration. However, we have used a more general expression (2.17) for the compressibility factor. More importantly, our results from § 2 allow us to calculate the drop in pressure across the particulate layer. Combining equations (2.4), (2.13) and (2.17) yields

$$\hat{p}(\hat{x}) = \hat{P} - \phi z(\phi), \tag{3.6}$$

where $\hat{p} = (v_p/k_B T)p$ and $\hat{P} = (v_p/k_B T)P$. Figure 6(*e–h*) shows plots of the drop in pervadic pressure corresponding to conditions in (*a–d*). In the Brownian limit (plots *a* and *e*) the pressure varies nonlinearly over the boundary layer, and the total drop in pressure experienced by the fluid is small. In the close-packed limit (plots *d* and *h*),

https://doi.org/10.1017/S0022112006009268 Published online by Cambridge University Press

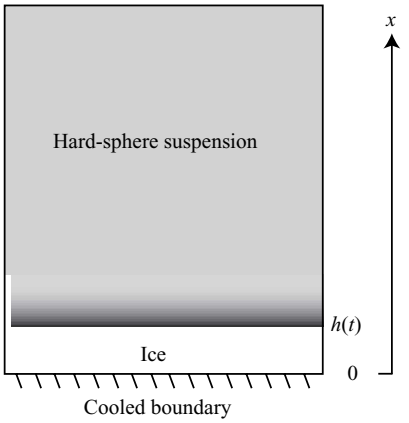


FIGURE 7. Unidirectional solidification of a hard-sphere suspension at initial temperature T_∞ and volume fraction ϕ_∞. The temperature at $x=0$ is reduced below the freezing temperature of the suspension. The ice rejects the particles, forming a concentrated boundary layer above the solidification front. The boundary layer is similar to the layer which forms during the filtration of a suspension of hard spheres in § 3.

$\mathrm{d}p/\mathrm{d}x$ is constant (as expected from the Darcy limit of a rigid porous medium) and the pressure drop is relatively large.

3.3. *Discussion*

The filtration of a suspension of hard spheres involves two distinct limits, corresponding to $Pe \sim 1$ (Brownian limit) and $Pe \gg 1$ (porous-medium limit). In the Brownian limit the system behaviour is similar to molecular diffusion in liquids: increasing the Péclet number causes the volume fraction at $\hat{x}=0$ to increase but does not significantly affect the shape of the $\phi(\hat{x})$ curve (figures 6*a* and 6*b*). However, as Pe continues to increase the particles near the filter approach the close-packing concentration ϕ_p. A layer of constant $\phi \approx \phi_p$ begins to form against the filter surface. For $Pe \gg 1$ the system behaviour is similar to flow through a porous medium.

In § 4.4 we find similar regimes during unidirectional solidification of a hard-sphere suspension. For small particles the system behaviour is similar to binary alloy solidification. However, for large particles a porous medium forms above the interface, and the behaviour is quite different.

4. Solidification of a hard-sphere suspension

Consider the system in figure 7. A hard-sphere suspension at initial volume fraction ϕ_∞ and temperature T_∞ is placed within a closed container. The temperature at the base is then reduced below freezing, and a layer of ice begins to grow upward from the boundary. We assume that the ice rejects all of the particles; i.e. the segregation coefficient $k_s \equiv \phi_s/\phi_i = 0$, where ϕ_s is the volume fraction of particles in the solid and ϕ_i is the volume fraction at the interface. We also neglect the effects of gravity and the expansion of ice on freezing. This is a model of the experimental system shown in figure 1(*a*).

4.1. *Extended Stefan equations*

In a closed system, conservation of mass of particles in the unfrozen suspension can be written

$$\frac{\partial \phi}{\partial t} = \frac{\partial}{\partial x} D(\phi) \frac{\partial \phi}{\partial x}. \tag{4.1}$$

https://doi.org/10.1017/S0022112006009268 Published online by Cambridge University Press

We choose here to describe transport in terms of the diffusivity D, to make comparisons with alloy solidification, though, as discussed earlier, the problem could be reformulated in terms of the permeability k. The boundary conditions are

$$\phi \to \phi_\infty \qquad (x \to \infty), \tag{4.2}$$

$$\phi \dot{h} = -D(\phi)\frac{\partial \phi}{\partial x} \qquad (x = h), \tag{4.3}$$

where $h(t)$ is the position of the solidification front and the dot denotes differentiation with respect to time.

We consider simple Fourier diffusion of heat with constant thermal properties of ice, water and particles, independent of phase, in which case the energy balance can be written

$$\frac{\partial T}{\partial t} = \kappa \frac{\partial^2 T}{\partial x^2}, \tag{4.4}$$

where $\kappa = k_T/\rho c_p$ is the thermal diffusivity, k_T is the thermal conductivity and c_p is the specific heat capacity. The boundary conditions on the temperature field are

$$T = T_b \quad (x = 0), \qquad \text{and} \qquad T \to T_\infty \quad (x \to \infty). \tag{4.5}$$

At the boundary $x = h(t)$ there is a Stefan condition expressing conservation of energy across the interface:

$$T = T_f(\phi), \qquad \rho L_f \dot{h} = k_T \left(\left.\frac{\partial T}{\partial x}\right|_{x=h^-} - \left.\frac{\partial T}{\partial x}\right|_{x=h^+} \right) \qquad (x = h), \tag{4.6}$$

where L_f is the latent heat of fusion, $T_f(\phi)$ is the thermodynamic freezing temperature, and the dot denotes differentiation with respect to time. To complete the description, an equation for the freezing temperature of a hard-sphere suspension is required.

4.2. *Freezing temperature*

An expression for the freezing temperature can be obtained by utilizing the conditions for local thermodynamic equilibrium between the suspension phase and the ice phase. Assuming the interface is planar and the phases are isotropically stressed, the temperature T, pressure P and chemical potentials μ_1 and μ_2 must be equal in both phases (Gibbs 1875, 1878). The condition for equality of μ_1 in both phases is

$$\mu_1^A = \mu_1^B, \tag{4.7}$$

where the superscripts A and B refer to the suspension and ice phases, respectively.

The chemical potential of component 1 in the suspension phase can be written (Prigogine & Defay 1954)

$$\mu_1^A = \mu^f(T, P) - \Pi(T, \phi)/\rho_f, \tag{4.8}$$

where μ^f is the chemical potential of pure fluid, Π is the osmotic pressure and ρ^f is the density of the pure fluid (assumed constant). A similar expression exists for the chemical potential of component 1 in the ice phase. If the ice phase is pure, however, the chemical potential is simply

$$\mu_1^B = \mu^i(T, P), \tag{4.9}$$

https://doi.org/10.1017/S0022112006009268 Published online by Cambridge University Press

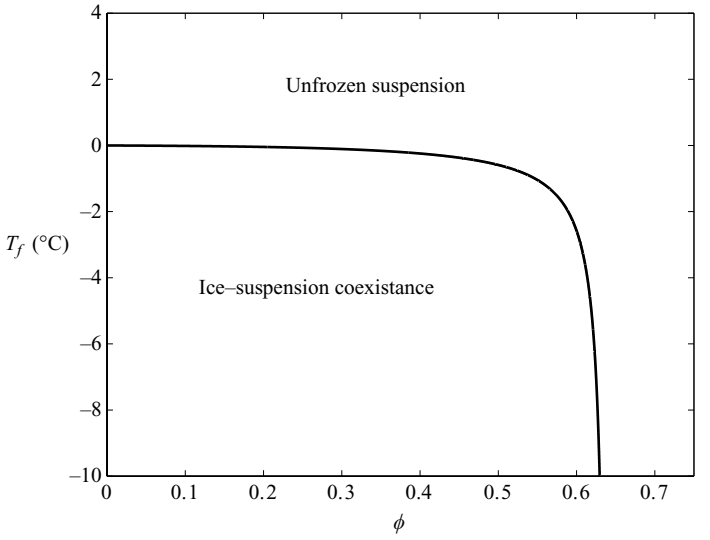


FIGURE 8. Freezing temperature of a suspension of hard spheres ($R = 2$ nm). When the temperature is above $T_f(\phi)$, the sample exists as a suspension. Below $T_f(\phi)$, ice and suspension can coexist, with the composition of the suspension determined by the freezing-temperature curve. Similar diagrams have been determined experimentally in food colloid systems (Roos 1995).

where μ^i is the chemical potential of pure ice. Inserting (4.8) and (4.9) into (4.7) yields, with (2.13),

$$\frac{\Pi}{T} = \frac{\phi}{v_p} k_B z(\phi) = \rho_f \frac{\mu^f - \mu^i}{T}. \tag{4.10}$$

Differentiating (4.10) with respect to T at constant P gives

$$\left(\frac{\partial \phi z}{\partial T}\right)_P = -\frac{\rho_f v_p L_f}{k_B T^2}, \tag{4.11}$$

where $L_f(T, P) = h^f - h^i$ is the latent heat and $h^f = \mu^f + T(\partial \mu^f / \partial T)_P$ the enthalpy per unit mass of fluid. For the relatively small temperature range of interest here, L_f can be taken as a constant and equation (4.11) integrated to yield

$$T_f = T_m(1 + m\phi z)^{-1}, \tag{4.12}$$

where T_m is the freezing temperature of the pure fluid and $m = k_B T_m / v_p \rho_f L_f$. Equation (4.12) is plotted in figure 8. The slope of the freezing-temperature curve approaches $-mT_m$ as $\phi \to 0$ and diverges near close packing. Note that m is inversely proportional to the particle volume v_p. That is, larger particles cause less depression of the freezing temperature for the same value of volume fraction.

In monodisperse hard-sphere suspensions another type of phase change, from suspension to colloidal crystal, can occur at high concentrations. At volume fractions higher than 0.49, hard-sphere colloids can arrange themselves into a crystalline structure (Russel *et al.* 1989; Van Megen *et al.* 1990). However, in many systems the colloidal crystal does not readily form (particularly if there is polydispersity in particle size) and the disordered suspension tends to persist as $\phi \to \phi_p$ (Russel *et al.* 1989; Auer & Frenkel 2001). In the present paper we study systems in which the colloidal crystal does not appear. Experimental freezing-temperature curves in

https://doi.org/10.1017/S0022112006009268 Published online by Cambridge University Press

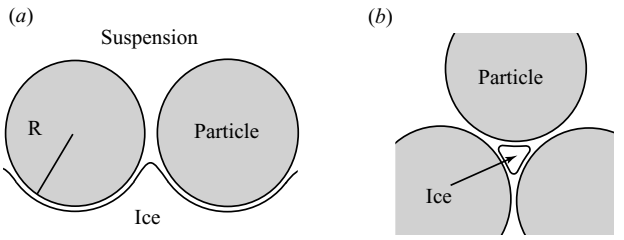


FIGURE 9. (*a*) Pore-scale view of the interface between ice and a close-packed suspension of hard spheres. (*b*) Plan view showing a pore throat through which ice can migrate if the temperature is sufficiently low.

colloidal systems show behaviour similar to the freezing-temperature curve in figure 8 (Simatos *et al.* 1975; Roos 1995).

Equation (4.12) gives the temperature at which ice is in local equilibrium with unfrozen suspension on the macroscopic scale. On this scale the ice–suspension interface is planar (figure 7). On the much smaller scale of a pore, however, the ice interface has a curvature (figure 9*a*) that depends on temperature. As the temperature decreases, the curvature will increase, eventually allowing ice to invade the pore space between particles (Kuhn, Peterli & Majer 1955; Scherer 1993). The freezing temperature curve will terminate at this 'ice-entry' temperature. In order to obtain an expression for the ice-entry temperature, we can apply thermodynamic conditions for equilibrium at the pore scale, following the approach of Kuhn *et al.* (1955) and Jackson & Chalmers (1958). The Gibbs–Thomson equation describing the freezing-point depression due to curvature of the ice in the space between the particles in figure 9 is (Liu *et al.* 2003; Rempel *et al.* 2004)

$$T - T_m = -\frac{T_m \gamma}{\rho_i L_f} \mathscr{K}, \tag{4.13}$$

where ρ_i is the density of ice, γ is the ice–water interfacial tension, and $\mathscr{K}$ is the mean curvature of the ice in the pore regions. The ice will enter the particle matrix when the curvature is greater than $2/r_p$ where r_p is the characteristic radius of a pore throat (figure 9*b*).

For a pore diameter of 1 μm equation (4.13) yields an ice-entry temperature of $T_I = -0.1\,^{\circ}\mathrm{C}$, while for a 1 nm pore, $T_I = -100\,^{\circ}\mathrm{C}$. Thus, for micron-sized particles, ice can enter the pores even at relatively warm temperatures, while for nanometre particles the ice is unlikely to enter the space between particles except at very low temperatures. For nanometre and smaller particles a glass transition may instead occur, terminating the freezing-temperature curve before the ice-entry temperature is reached (Simatos *et al.* 1975; Roos 1995).

If the temperature at the interface reaches the ice-entry temperature, the ice will engulf the particles. Alternatively, if local equilibrium fails at the interface due to rapid freezing, the particles may be engulfed at warmer temperatures via the effect of interfacial viscous forces (Uhlmann *et al.* 1964; Worster & Wettlaufer 1999). In the present work we consider sufficiently slow freezing and relatively warm temperatures such that local equilibrium prevails and the temperature at the interface is given by equation (4.12).

https://doi.org/10.1017/S0022112006009268 Published online by Cambridge University Press

4.3. *Similarity solution*

Equations (4.1) to (4.6) admit a similarity solution (Rubinstein 1971; Huppert & Worster 1985; Worster 2000) with variable

$$\eta = \frac{x}{(4D_0 t)^{1/2}} \tag{4.14}$$

and interface position

$$h(t) = 2\lambda(D_0 t)^{1/2}, \tag{4.15}$$

where λ is a constant. Introducing the above similarity variables, along with the Stefan number

$$St = \frac{L_f}{\rho c_p (T_\infty - T_f(\phi_\infty))}, \tag{4.16}$$

the Lewis number

$$Le = \frac{\kappa}{D_0}, \tag{4.17}$$

and the dimensionless temperature

$$\theta = \frac{T - T_\infty}{T_f(\phi_\infty) - T_\infty}, \tag{4.18}$$

yields the system of ordinary differential equations

$$\frac{\mathrm{d}\phi}{\mathrm{d}\eta} = -\frac{1}{2\eta}\frac{\mathrm{d}}{\mathrm{d}\eta} D(\phi)\frac{\mathrm{d}\phi}{\mathrm{d}\eta}, \tag{4.19}$$

$$\frac{\mathrm{d}\theta}{\mathrm{d}\eta} = -\frac{Le}{2\eta}\frac{\mathrm{d}^2\theta}{\mathrm{d}\eta^2}, \tag{4.20}$$

with boundary conditions

$$\phi \to \phi_\infty, \qquad \theta \to 0 \qquad (\eta \to \infty), \tag{4.21}$$

$$\phi = 0, \qquad \theta = \theta_b \qquad (\eta = 0), \tag{4.22}$$

$$\phi = \phi_h, \qquad \phi\lambda = \frac{1}{2} D(\phi)\frac{\mathrm{d}\phi}{\mathrm{d}\eta}\bigg|_{\eta=\lambda^+} \qquad (\eta = \lambda), \tag{4.23}$$

$$\theta = \theta_h, \qquad \lambda = -\frac{Le}{2St}\left(\frac{\mathrm{d}\theta}{\mathrm{d}\eta}\bigg|_{\eta=\lambda^-} - \frac{\mathrm{d}\theta}{\mathrm{d}\eta}\bigg|_{\eta=\lambda^+}\right) \qquad (\eta = \lambda), \tag{4.24}$$

$$\theta_h = \theta_m + \Gamma\left(\frac{\phi_h z(\phi_h)}{1 + m\phi_h z(\phi_h)}\right), \tag{4.25}$$

where $\Gamma = mT_m/(T_\infty - T_f(\phi_\infty))$.

For $0 \leqslant \eta < \lambda$ the equations above yield the analytical solution (Carslaw & Jaeger 1959; Worster 1986)

$$\phi = 0, \tag{4.26}$$

$$\theta = \theta_b + \left(\frac{T_h - T_b}{T_f(\phi_\infty) - T_\infty}\right)\frac{\mathrm{erf}\left(Le^{-1/2}\eta\right)}{\mathrm{erf}\left(Le^{-1/2}\lambda\right)}. \tag{4.27}$$

For $\eta > \lambda$ the equations can be solved numerically using the shooting method.

https://doi.org/10.1017/S0022112006009268 Published online by Cambridge University Press

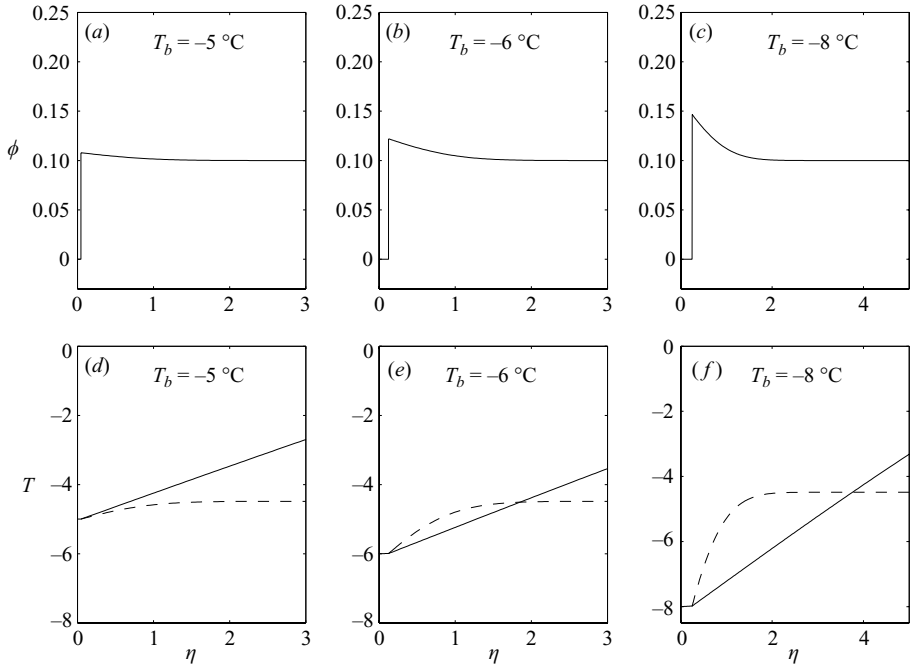


FIGURE 10. Volume fraction and temperature profiles during the unidirectional solidification of a hard-sphere suspension ($Le = 250$, $mT_m = 30\,^\circ$C, $T_\infty = 6\,^\circ$C, and $\phi_\infty = 0.1$). Similar profiles are seen during the solidification of binary alloys (Worster 2000; Davis 2001). The actual temperature (solid line) in (*e*) and (*f*) is lower than the freezing temperature (dashed line) and the suspension is constitutionally supercooled.

4.4. *Solidification profiles*

Equations (4.19)–(4.25) were integrated using the MATLAB ODE Suite (Shampine & Reichelt 1997). Figures 10 and 11 show solutions of the equations for different values of the Lewis number Le, the temperature T_b at the base, and the freezing-temperature parameter m. The Lewis number $Le = \kappa/D_0$ plays a similar role to the Péclet number $Pe = qL\phi_0/D_0$ of § 3. At relatively small values of the Lewis number, the velocity of the interface (controlled by the rate of heat transfer) tends to be small compared to the velocity at which the particles can migrate by Brownian diffusion. For large enough values of Le, however, Brownian motion is weak, and the particles tend to form a close-packed layer (porous medium) above the interface.

The parameters used in figure 10 ($Le = 250$, $mT_m = 30\,^\circ$C, $T_\infty = 6\,^\circ$C, $\phi_\infty = 0.1$, $St = 20$, $\Gamma = 5$) were chosen to illustrate the analogy with alloy solidification (Worster 2000; Davis 2001). For a Lewis number of 250, Brownian diffusion is quite strong (for 1 nm particles in water equation (4.17) yields a Lewis number of approximately 250). The driving force for solidification is the undercooling at the base, $\Delta T = T_b - T_f(\phi_\infty)$. At relatively slow solidification rates (figure 10(*a*), where $\Delta T = -0.5\,^\circ$C) the particles easily diffuse away from the interface. The temperature of the suspension ahead of the interface (represented by the solid line in figure 10(*d*)) is always warmer than the freezing temperature (the dashed line). However, at faster solidification rates the concentration and concentration gradient increase at the interface. In figure 10(*e*) the concentration gradient at the interface is steep enough that the gradient in the freezing temperature is larger than the temperature gradient, and the suspension ahead of

https://doi.org/10.1017/S0022112006009268 Published online by Cambridge University Press

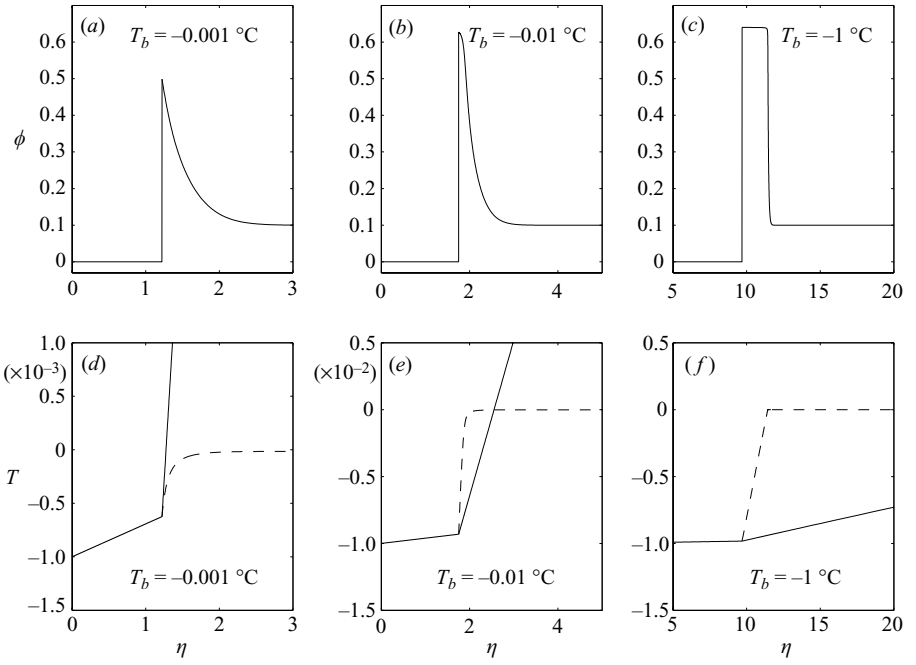


FIGURE 11. Volume fraction and temperature profiles during the unidirectional solidification of a hard-sphere suspension ($Le = 10^4$, $mT_m = 10^{-4}$ °C, $T_\infty = 1$ °C, and $\phi_\infty = 0.1$). In this case the particles experience less Brownian diffusion, and can form a porous medium against the ice–suspension interface (*c*). The actual temperature (solid line) in (*e*) and (*f*) is lower than the freezing temperature (dashed line) and the suspension is constitutionally supercooled. If the porous medium is stable, ice could nucleate in the supercooled region ahead of the porous layer.

the interface is below its freezing temperature (constitutionally supercooled). In the case of binary alloys, constitutional supercooling is closely related to morphological instability (Mullins & Sekerka 1964; Davis 2001), and the interface will tend to deform into the supercooled region.

In figure 11, $Le = 10^4$, and $mT_m = 10^{-4}$ °C. In this case the particles are larger ($R = 15$ nm), and experience less Brownian motion. The smaller value for m has been estimated based on equation (4.12): it reflects the expectation that large particles cause less depression of the freezing temperature. If the solidification rate is sufficiently slow ($\Delta T = -0.001$ °C in figure 11(*a*)), the particles can still diffuse away from the interface. At higher solidification rates (figure 11(*b*)), the particles build up against the interface forming a layer of nearly constant volume fraction (figure 11(*c*)). The freezing temperature varies approximately linearly over the porous medium, with the maximum in supercooling occurring near the surface of the layer. If the porous medium remains stable during the buildup, secondary nucleation of ice could occur at the position of maximum supercooling.

4.5. *Discussion*

As in the case of filtration (§ 3), the solidification of a suspension of hard spheres involves two distinct limits, corresponding to small particles (Brownian limit) and large particles (porous-medium limit). In the Brownian limit, the system's behaviour is similar to alloy solidification. A diffuse boundary layer builds up against the solidification front and can cause the suspension ahead of the ice front to become

https://doi.org/10.1017/S0022112006009268 Published online by Cambridge University Press

supercooled. In this case the interface can become unstable, forming cellular structures which preferentially grow into the supercooled region.

In the porous-medium limit, a compact layer of nearly uniform concentration forms against the freezing front. The porous medium is then supercooled, allowing for the possibility of a morphological instability. Experiments in our laboratory have revealed such an instability, as well as the subsequent growth of ice dendrites, during the unidirectional solidification of montmorillonite clay (figure 1). In other systems (for example a rigid, connected porous medium) the porous matrix may remain stable. In this case there exists the possibility that ice could nucleate in the supercooled region ahead of the porous layer. This type of behaviour is thought to have occurred during the freezing of a microporous filter (Ozawa & Kinosita 1989), articular cartilage (Muldrew *et al.* 2000) and Portland cement paste (Corr *et al.* 2003), and may explain the behaviour illustrated in figure 2.

In the experiments of Mutou *et al.* (1998), during which a suspension of silica particles was unidirectionally frozen, the freezing interface remained planar while a compact layer of particles formed ahead of the freezing front. The interface then appeared to undergo a series of instabilities, involving first the capture of particles along grain boundaries, and finally the engulfment of the entire layer by the ice (K. Watanabe 2004, personal communication). Similar observations were made by Mashl *et al.* (1996), who studied the unidirectional solidification of a suspension of starch particles. One potential explanation for the engulfment of the particles is that the ice-entry temperature was reached, as discussed in § 4.2. Another possibility is that the segregation coefficient $k_s = \phi_s/\phi_i$ is not always zero (as assumed in this section) but depends on the interface velocity, with $k_s(\dot{h}) \to 1$ as $\dot{h}$ approaches the critical engulfment velocity (Uhlmann *et al.* 1964; Worster & Wettlaufer 1999). This could lead to an oscillatory instability (Coriell & Sekerka 1983) and particle engulfment at high velocities.

Although we have not undertaken a stability analysis here, it is hoped that the present theory provides a basic framework for modelling freezing phenomena in colloidal systems. In future, linear and nonlinear stability analyses may be found useful in providing a deeper understanding of these systems.

5. Conclusion

We have developed equations describing the unidirectional solidification of a suspension of hard-sphere particles. For very small particles Brownian diffusion is important and the concentration and temperature profiles resemble those observed during alloy solidification. In certain cases, the interface can become unstable owing to constitutional supercooling. For larger particles Brownian diffusion is weak or absent and a porous medium forms against the freezing front. The porous medium is supercooled, allowing for the possibility of a morphological instability. If the porous medium is stable ice could nucleate in the supercooled suspension ahead of the porous layer. The interplay between these mechanisms could explain some of the great variety of freezing patterns observed in soils, tissue, and other colloidal materials.

We thank John Wettlaufer and Kunio Watanabe for several helpful discussions. We also thank the anonymous referees for their insightful comments. S. S. L. Peppin was sponsored by a Gates Cambridge Scholarship and a grant from Trinity College. J. A. W. Elliott holds a Canada Research Chair in Interfacial Thermodynamics. This research was additionally supported by a grant from the Leverhulme Trust.

https://doi.org/10.1017/S0022112006009268 Published online by Cambridge University Press

REFERENCES

Auer, S. & Frenkel, D. 2001 Suppression of crystal nucleation in polydisperse colloids due to increase of the surface free energy. *Nature* **413**, 711–713.

Auzerais, F. M., Jackson, R. & Russel, W. B. 1988 The resolution of shocks and the effects of compressible sediments in transient settling. *J. Fluid Mech.* **195**, 437–462.

Batchelor, G. K. 1976 Brownian diffusion of particles with hydrodynamic interactions. *J. Fluid Mech.* **74**, 1–29.

Black, P. B. 1991 Historical perspective of frost heave research. *CRREL Special Rep.* 91–23, pp. 3–7.

Brady, J. F. 1993 Brownian motion, hydrodynamics, and the osmotic pressure. *J. Chem. Phys.* **98**, 3335–3341.

Carnahan, N. F. & Starling, K. E. 1969 Equation of state for nonattracting rigid spheres. *J. Chem. Phys.* **51**, 635–636.

Carslaw, H. S. & Jaeger, J. C. 1959 *Conduction of Heat in Solids*. Oxford University Press.

Chernov, A. A., Temkin, D. E. & Mel'nikova, A. M. 1976 Theory of the capture of solid inclusions during the growth of crystals from the melt. *Sov. Phys. Crystallogr.* **21**, 369–374.

Coriell, S. R. & Sekerka, R. F. 1983 Oscillatory morphological instabilities due to non-equilibrium segregation. *J. Cryst. Growth* **61**, 499–508.

Corr, D. J., Monteiro, P. J. M & Bastacky, J. 2003 Observations of ice lens formation and frost heave in young Portland cement paste. *Cem. Concr. Res.* **33**, 1531–1537.

Davis, K. E. & Russel, W. B. 1989 An asymptotic description of transient settling and ultrafiltration of colloidal dispersions. *Phys. Fluids* A **1**, 82–100.

Davis, K. E., Russel, W. B. & Glantschnig, W. J. 1989 Disorder-to-order transition in settling suspensions of colloidal silica: X-ray measurements. *Science* **245**, 507–510.

Davis, S. H. 2001 *Theory of Solidification*. Cambridge University Press.

Gibbs, J. W. 1875/1878 On the equilibrium of heterogeneous substances. *T. Conn. Acad. Sci.* **3**, 108–248, 343–524.

Huppert, H. E. 1990 The fluid mechanics of solidification. *J. Fluid Mech.* **212**, 209–240.

Huppert, H. E. & Worster, M. G. 1985 Dynamic solidification of a binary melt. *Nature* **314**, 703–707.

Jackson, K. A. & Chalmers, B. 1958 Freezing of liquids in porous media with special reference to frost heave in soils. *J. Appl. Phys.* **29**, 1178–1181.

Kuhn, W., Peterli, E. & Majer, H. 1955 Freezing point depression of gels produced by high polymer network. *J. Polym. Sci.* **16**, 539–548.

Kurz, W. & Fisher, D. J. 1986 *Fundamentals of Solidification*. Trans. Tech. Publications.

Liu, Z., Muldrew, K., Wan, R. G. & Elliott, J. A. W. 2003 Measurement of freezing point depression of water in glass capillaries and the associated ice front shape. *Phys. Rev.* E **67**, 061602.

McMillan, W. G. & Mayer, J. E. 1945 Statistical mechanics of multicomponent systems. *J. Chem. Phys.* **13**, 276–305.

McQuarrie, D. A. 1986 *Statistical Mechanics*. Harper & Row.

Mashl, S. J., Flores, R. A. & Trivedi, R. 1996 Dynamics of solidification in 2% corn starch-water mixtures: Effect of variations in freezing rate on product homogeneity. *J. Food Sci.* **61**, 760–765.

Miller, R. D. 1972 Freezing and heaving of saturated and unsaturated soils. *Highway Res. Rec.* **393**, 1–11.

Muldrew, K., Novak, K., Yang, H., Zernicke, R., Schachar, N. S. & McGann, L. E. 2000 Cryobiology of articular cartilage: Ice morphology and recovery of chondrocytes. *Cryobiology* **40**, 102–109.

Mullins, W. W. & Sekerka, R. F. 1964 Stability of a planar interface during solidification of a dilute binary alloy. *J. Appl. Phys.* **35**, 444–451.

Mutou, Y., Watanabe, K., Ishizaki, T. & Mizoguchi, M. 1998 Microscopic observation of ice lensing and frost heave in glass beads. *Proc. 7th Intl Conf. on Permafrost, Yellowknife, Canada; Centre d'Études Nordique, Université Laval, Canada*, pp. 783–787.

O'Neill, K. & Miller, R. D. 1985 Exploration of a rigid ice model of frost heave. *Water Resour. Res.* **21**, 281–296.

https://doi.org/10.1017/S0022112006009268 Published online by Cambridge University Press

Ozawa, H. & Kinosita, S. 1989 Segregated ice growth on a microporous filter. *J. Colloid Interface Sci.* **132**, 113–124.

Peppin, S. S. L., Elliott, J. A. W. & Worster, M. G. 2005 Pressure and relative motion in colloidal suspensions. *Phys. Fluids* **17**, 053301.

Petsev, D. N., Starov, V. M. & Ivanov I. B. 1993 Concentrated dispersions of charged colloidal particles: sedimentation, ultrafiltration and diffusion. *Coll. Surf.* A **81**, 65–81.

Prigogine, I. & Defay, R. 1954 *Chemical Thermodynamics.* Longmans, Green & Co.

Rallison, J. R. 1988 Brownian diffusion in concentrated suspensions of interacting particles. *J. Fluid Mech.* **186**, 471–500.

Ree, F. H. & Hoover, W. G. 1964 Fifth and sixth virial coefficients for hard spheres and hard disks. *J. Chem. Phys.* **40**, 939–950.

Rempel, A. W., Wettlaufer, J. S. & Worster, M. G. 2004 Premelting dynamics in a continuum model of frost heave. *J. Fluid Mech.* **498**, 227–244.

Rempel, A. W. & Worster, M. G. 1999 The Interaction between a particle and an advancing solidification front. *J. Cryst. Growth* **205**, 427–440.

Rintoul, M. D. & Torquato, S. 1996 Computer simulations of dense hard-sphere systems. *J. Chem. Phys.* **105**, 9258–9265.

Roos, Y. H. 1995 *Phase Transitions in Foods.* Academic.

Rubinstein, L. I. 1971 *The Stefan Problem.* American Mathematical Society Translation No. 27, American Mathematical Society, Providence.

Russel, W. B., Saville, D. A. & Schowalter, W. R. 1989 *Colloidal Dispersions.* Cambridge University Press.

Scherer, G. W. 1993 Freezing gels. *J. Non-Cryst. Solids* **155**, 1–25.

Shampine, L. F. & Reichelt, M. W. 1997 The MATLAB ODE suite. *SIAM J. Sci. Comput.* **18**, 1–22.

Simatos, D., Faure, M., Bonjour, E. & Couach, M. 1975 The physical state of water at low temperatures in plasma. *Cryobiology* **12**, 202–208.

Taber, S. 1929 Frost heaving. *J. Geol.* **34**, 428–461.

Thiele, E. 1963 Equation of state for hard spheres. *J. Chem. Phys.* **39**, 474–479.

Uhlmann, D. R., Chalmers, B. & Jackson, K. A. 1964 Interaction between particles and a solid/liquid interface. *J. Appl. Phys.* **35**, 2986–2992.

Van Megen, W., Pusey, P. N. & Bartlett, P. 1990 Phase behavior of dispersions of hard spherical particles. *Phase Transit.* **21**, 207–227.

Watanabe, K. 2002 Relationship between growth rate and supercooling in the formation of ice lenses in a glass powder. *J. Cryst. Growth* **237-239**, 2194–2198.

Watanabe, K. & Mizoguchi, M. 2000 Ice configuration near a growing ice lens in a freezing porous medium consisting of micro glass particles. *J. Cryst. Growth* **213**, 135–140.

Watanabe, K., Muto, Y. & Mizoguchi, M. 2001 Water and solute distributions near an ice lens in a glass-powder medium saturated with sodium chloride solution under unidirectional freezing. *Cryst. Growth Des.* **1**, 207–211.

Woodcock, L. V. 1981 Glass transition in the hard-sphere model and Kauzmann's paradox. *Ann. New York Acad. Sci.* **371**, 274–298.

Worster, M. G. 1986 Solidification of an alloy from a cooled boundary. *J. Fluid Mech.* **167**, 481–501.

Worster, M. G. 2000 Solidification of fluids. In *Perspectives in Fluid Dynamics* (ed. G. K. Batchelor, H. K. Moffatt & M. G. Worster), pp. 393–446. Cambridge University Press.

Worster, M. G. & Wettlaufer, J. S. 1999 The fluid mechanics of premelted liquid films. In *Fluid Dynamics at Interfaces* (ed. W. Shyy). Cambridge University Press.

Zhang, H., Hussain, I., Brust, M., Butler, M. F., Rannard, S. P. & Cooper, A. I. 2005 Aligned two- and three- dimensional structures by directional freezing of polymers and nanoparticles. *Nature Mat.* **4**, 787–793.

https://doi.org/10.1017/S0022112006009268 Published online by Cambridge University Press